SOS

Isolated health monitoring system to save our satellites

Narayana, Sujay; Prasad, R. Venkatesha; Prabhakar, T. V.

DOI
10.1145/3458864.3466862

Publication date
2021

Document Version
Final published version

Published in
MobiSys 2021 - Proceedings of the 19th Annual International Conference on Mobile Systems, Applications, and Services

SOS: Isolated Health Monitoring System to Save Our Satellites

Sujay Narayana
Delft University of Technology
The Netherlands
sujay.narayana@tudelft.nl

R. Venkatesha Prasad
Delft University of Technology
The Netherlands
r.r.venkateshaprasad@tudelft.nl

T. V. Prabhakar
Indian Institute of Science
India
tvprabs@iisc.ac.in

ABSTRACT

With the advent of Space-IoTs, the rate of launch of satellites has grown significantly. Alongside, the failure rate of satellites has also surged increased tremendously. Satellites are non-repairable systems in orbit, and the financial loss incurred when the satellites fail before their expected mission time is substantial. If the source of a failure is known while the satellite is in orbit, then there is a possibility to revive it by sending appropriate commands from ground stations. In this work, we present a simple, independent satellite health monitoring system called Chirper. The Chirper is equipped with multiple modules such as IMU, isolated voltage and current measurement probes, and an onboard communication channel. We present a new approach to measure low DC voltages in an isolated way, providing a resolution and accuracy of around 1 V. We evaluated the design and performance of the Chirper through simulation, testing it in space systems test facility, and by mounting it on a helium balloon. With extensive experiments we show that 90% of the time the dc voltage measurement error is within 0.8 V, and the maximum error is 0.9 V. We expect to launch the Chirper soon on a space system.

CCS CONCEPTS

• **Computer systems organization** → **Embedded hardware**; • **Hardware** → **Sensors and actuators**; **Wireless devices**.

ACM Reference Format:
Sujay Narayana, R. Venkatesha Prasad, and T. V. Prabhakar. 2021. SOS: Isolated Health Monitoring System to Save Our Satellites. In *The 19th Annual International Conference on Mobile Systems, Applications, and Services (MobiSys '21), June 24-July 2, 2021, Virtual, WI, USA.* ACM, New York, NY, USA, 13 pages.

1 INTRODUCTION

In the recent years, the rate of launch of satellites has grown significantly – mainly due to innovations in space vehicles and advancements in miniaturized space systems. Alongside successful launch missions, the failure rate of satellites has also surged significantly. According to NASA, a whopping 35.2% of the satellites launched between the years 2000 and 2016 have failed completely [1] (see **Figure 1**). Of these failures, the causes of breakdown are unknown for 16% of the satellites despite planned redundant systems. Further, the failure rate was increased to 43% between the years 2009 and 2016 as shown in **Figure 1**. Studies also show that ≈41% of the satellites failed within one year after launch [2]. If the reasons for failures are known, then the satellite may be revived (to some extent) by sending appropriate commands from the ground station. Further, such failures can be avoided in future satellites.

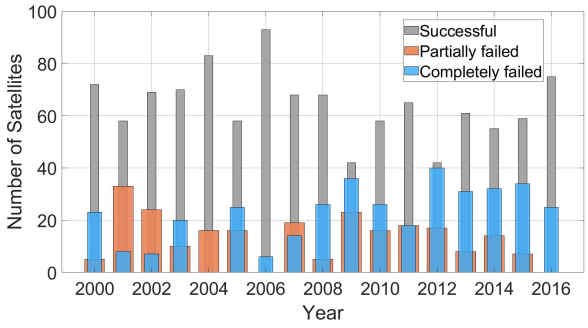

Figure 1: Percentage of small satellites launched and the failure rate since 2000; both rates have grown significantly (NASA statistics).

How can a failed satellite be revived? In most of the cases, if the source of failure can be identified, then the satellite may be saved by telecommanding from the ground station. For instance, one of the basic subsystems used in satellites is a star tracker that helps in determining the attitude of the satellite precisely from the visible star positions. Star tracker helps payloads such as a high definition camera that require precise pointing. If it is possible to identify that the star tracker is not functional, then the satellite can be revived by turning it off and rely on gyroscope and magnetometer for attitude determination at the cost of measurement accuracy. Indeed, most of the satellites have multiple health monitoring self-help capabilities and regularly transmit housekeeping data, such as primary satellite bus voltage, current, and status of different subsystem, to the ground station over its communication channel. Hence, any indication of the subsystem failures can be known. While most of these solutions are based on onboard software diagnostics, information needs to be transmitted to the ground station using the same hardware present onboard. However, if the communication system fails to operate, then the reasons for failure stay unexplained. Thus, in this paper, we propose a simple, self-powered, independent, and miniaturized module called Chirper that can provide a secondary channel for the health monitoring system for satellites for ≈ 250US$. The name Chirper symbolizes the sound a bird makes when it faces a dangerous situation. Chirper can track the satellite health parameters at regular intervals and then transmit them to the ground station independently. Depending on the causes for failure, further action can be taken by the satellite manufacturers to save the satellite.

MobiSys '21, June 24-July 2, 2021, Virtual, WI, USA © 2021
Copyright held by the owner/author(s).
ACM ISBN 978-1-4503-8443-8/21/07.
https://doi.org/10.1145/3458864.3466862

How can Chirper save a satellite?

A satellite can have both hardware and software based onboard fault detection systems and they can intimate the source of failure to the ground stations via onboard communication channel [3–5]. However, if the main power system or the communication channel is faulty, then there is no means to identify the cause of the failure, or to revive the satellite. According to the literature, 45% of the failures in satellites are caused by the fault in electronics. While 32% of the electronic faults are due to the failure in Attitude Determination and Control System (ADCS)[1], 27% is from the power system, 12% from the communication system, and 16% due to unknown reasons [1, 2]. A few failures can also be interdependent on different subsystems of the satellite. For instance, there may be unexpected tumbling due to a failure in attitude control subsystem. Due to this, the power system can get affected as solar panels are not pointed towards the Sun continuously. For more details on the satellites that failed due to different reasons and the causes of different failures, we point the readers to [1, 2]. Chirper is capable of monitoring the source of major faults in a satellite that can arise due to unexpected voltage/current consumption levels, unforeseen tumbling, and thermal issues.

Chirper is equipped with multiple isolated voltage and current measurement probes. These probes are capable of measuring both voltage and current consumption of different satellite subsystems in real-time and transmit the information to the ground station directly with its onboard communication module. Further, Chirper also embeds a low-power 9 Degrees of Freedom (DoF) Inertial Motion Unit (IMU) to measure other critical statuses of the satellite, such as tumbling (spinning) rate and attitude of the satellite (see **Figure 2**). The thermistors placed at different locations of a satellite connected to the Chirper using wires measure the temperature on those locations, thus modelling the thermal information. When a satellite is in distress, the information provided by the Chirper can aid in diagnosing the fault.

All these health parameters are transmitted at regular intervals to the ground stations over a low-power long-range onboard communication channel. If any of the subsystems under supervision behave abnormally leading to power setbacks, under-voltage and line shorts, unexpected tumbling rate, communication system blackout, or other issues, then the information received from Chirper at the ground stations can aid the satellite manufacturer to take further steps to save the satellite as early as possible. Even if there is faint telemetry from the satellite (a case when communication system malfunctions and the radio does not transmit signals at the required power level) that is not being detected by the ground stations, the Chirper can sense those signals, or even decode them if the transmission frequency of the satellite is within Chirper's supported range. Further, Chirper is completely independent in its operation and electrically isolated from the satellite (parent). Hence, any damage in the subsystems of the satellite will not harm the Chirper, and the failure can be indirectly diagnosed without it being a part of the satellite. The complete isolation also ensures the safe and independent operation of the Chirper providing redundancy in health monitoring.

[1]ADCS comprises of sensors such as Inertial Motion Unit (IMU), star tracker, GPS module, magnetorquers, and reaction wheels

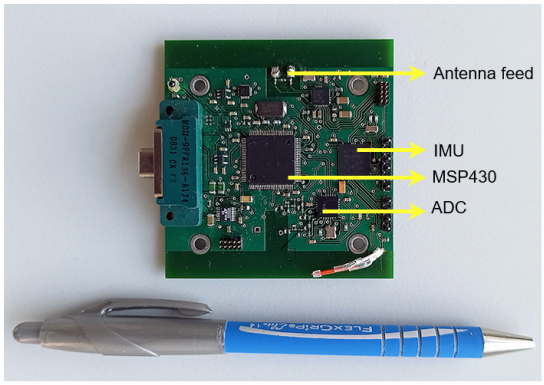

Figure 2: Chirper, a simple, self-powered, independent and miniaturized satellite health monitoring system for satellites.

While Chirper is designed only to detect faults and monitor the satellite, it cannot fix the problem on the satellite on its own. However, the data received from it can aid in retrieving failed satellites. Additionally, the received information has substantial weight in portraying the lessons learned to modify future designs to avoid such problems. To the best of our knowledge, we are the first to provide such an independent, completely isolated hardware-based satellite health monitoring system with the aforementioned features. The functionality can be expanded by allowing Chirper to communicate with the parent satellite (say, via a wireless link) so that emergency telecommanding could be done via the Chirper itself.

In this paper, we not only present the design principles and working of the Chirper but also provide insights into the common failures of satellites, Chirper design choices, and in-depth evaluation.

Motivation. The work presented in this paper was necessitated because a satellite, SAT-1[2], launched in 2019 malfunctioned leading to the mission failure. The satellite had a high definition infrared camera as a primary payload, and its main mission was to capture photos of Earth at night (anti-sun-lit side of Earth). The satellite worked only for a few hours after the launch, and there was no signal from the satellite for a few days. The cause of the failure was unknown. Twenty days later, there was a transmission from the satellite. From the telemetry received, it was identified that the heater system got damaged, and it was consuming all the available power from the battery as it went non-functional around four hours after the launch. The main bus voltage had dropped to 8 V from 48 V. Due to this, the battery drained intermittently, and the discharge cycle count crossed the allowed threshold, spoiling the battery. Now, with the heater system and battery completely dead, the satellite is functional only when there is sunlight as the solar panel is intact but the primary mission was declared a failure leading to a loss of $20 M. The heater system was optional, and even without it, the satellite would have been functional. If there was a system that was independent of the electric power from the satellite, that could send the status of different subsystems (in this case, mainly the heater

[2]the satellite name is not mentioned due to the restrictions from the satellite manufacturer

power consumption) of the satellite to the ground station, then the optional heater system could have been turned off immediately by sending commands to save the satellite.

Apart from SAT-1, many other expensive satellites, such as Boeing's Intelsat 29e [6] costing anywhere between $400 and $450 M, failed in 2019 due to unknown damage. GSAT 6A worth $36 M launched in April 2018 [7] failed while firing to geostationary orbit, the cause still being unknown.

Contributions. Our contributions are of several folds:

(**1**) In this work, we present a novel design of a miniaturized, low-cost, hardware-based isolated health monitoring system for satellites. To the best of our knowledge, we are the first to provide such a solution.

(**2**) We implemented Chirper in a small form-factor (5 cm x 4 cm, 32 g) by employing simple sensing and processing units using high reliability space-qualified components. The design will be open-source so that it can be highly beneficial to the entire space community.

(**3**) We propose a novel methodology and a model to measure low DC voltage based on capacitive technology that does not need any electrical contact for measurement. We are the first to provide such an isolated voltage measurement solution and this technique can be used not only in the space domain but also in terrestrial applications.

(**4**) The proposed Chirper design is retrospective. It is flexible to be mounted anywhere inside or on the body of the satellites, almost of any size. No customization or additional testing is required on the satellite.

(**5**) We conducted extensive performance evaluations of Chirper with simulation (for isolated DC voltage measurement) and real-time testing by mounting it on an actual satellite. Further, by launching it on a high altitude balloon[3], we show that Chirper is functional even when it is tumbling (when the harvested power is intermittent).

2 ON FAILURES, REQUIREMENTS FOR THE CHIRPER DESIGN

Before proceeding with the design of Chirper, it is crucial to know the cause of critical breakdowns in majority of the satellites. With this knowledge, Chirper can be equipped with specific components and features to detect these failures. These requirements were elicited from the known cases of the satellite failures since 2000 [1, 2].

2.1 Major causes of failures in satellites

Mechanical or thermal failures. The structural failure in a satellite is mainly caused by the collision with space debris. Debris detection is out of the context of this work. Mechanical failures are caused by unexpected faults in thermal mechanics (extreme heat and cold damaging electronics), and external forces such as solar flares. Thermal control is one of the crucial aspects of satellite development. The outer body temperature of a satellite can go as high as 123° C to as low as -170° C depending on its orbit, and it is important to maintain the temperature of electronics inside the satellite within their operating range [2, 8]. Failing to do so can damage the electronics system severely, leading to the loss of mission. Out of the satellite failures between 1980 and 2005, 32% of them were caused by mechanical or thermal failures [2].

Electronics. A survey from S. Tafazoli shows that almost 45% of the mission failures are caused by the fault in electronics [2]. There are many reasons for electronics failure:
(1) If the active thermal control systems such as heaters fail to maintain the required temperature inside the satellite, the electronic components may stop working. Especially, the battery is the most affected component in a satellite due to thermal system failures as they have a smaller operating range (0 - 60° C typically).
(2) With the advent of Space Internet of Things[9] and satellite constellations, there is a lot of interest for small satellites that are developed using Commercially Off The Shelf (COTS) components as they speed up the manufacturing lead time, cost, and increase productivity [8–11]. However, most of the COTS components used in small satellites may not be tested to work for a long duration in the space environment. COTS electronics in space have a higher chance of failure and swift performance degradation than space-grade components. Unlike COTS, space-grade electronics are radiation-hardened and support higher operating temperature range of -55° C to 125°C.
(3) Radiations in space can cause (a) Single Event Upsets (SEU), which is the change of state caused by single ionizing particle such as ions, electrons, photons striking a sensitive node in an electronic device. (b) Single Event Latchups (SEL), which is a type of short circuit that can occur in an integrated circuit. In non-space-grade electronics components, SEU and SEL may lead to temporary or permanent damage to the subsystems.

Unexpected tumbling. When a satellite is ejected from the deployer, it starts tumbling (spinning) in random directions. The tumbling rate and orientation depend on the force and course at which the deployer ejects the satellite. Especially in the case of deployable solar configuration, it is essential to point the solar panels towards the Sun by detumbling the satellite as quickly as possible to charge the batteries. If not, the batteries may be undercharged due to intermittent solar light. The stabilization of the satellite is carried out by the Attitude Determination and Control Systems (ADCS) in the satellites that can frequently fail [1, 2], leading to intermittent or no communication, or exhausting battery charge/discharge cycles. There are also many instances where Inertial Motion Sensors (IMUs) fail to sense the exact tumbling rate in three axes, leading to mission failure resulting in a loss of millions of dollars [2, 12, 13]. Chirper can independently estimate the tumbling rate of the satellite using its onboard IMU.

Software. Software failures are caused mainly because of software bugs that are undetected during testing, or the scenario that caused the bug was not reproducible on the ground during the trial. Additionally, blind and erroneous telecommands sent to the satellite can also introduce software bugs. We do not elaborate on the software bugs as it is out of the context of this work.

Non-standard failures. Apart from the aforementioned failures, the source of other not so frequent failures is next to impossible to pinpoint. It is also not possible to retrieve telemetry to investigate the reasons for a breakdown if there is a critical failure in the main power or communication subsystem. As per a survey from NASA,

[3]The Chirper was stipulated to be launched in mid-2020 but it was put off due to the current situation.

the reasons for failure are unknown for 16% of the total satellites failed between 2000 and 2016 [1].

2.2 Design Requirements

Analyzing the major failure causes in satellites, the detection system developed must have certain hardware/software requirements. **R.1:** the utmost requirement is that the system must be electrically isolated from the satellite completely. This is to ensure that any malfunction (such as electrical short) in the Chirper should not damage the rest of the satellite. **R.2:** it should be possible to monitor the supply voltage and current consumption of subsystems and payloads in an isolated way. **R.3:** the system should have its own power system to avoid leeching on the satellite's power system. **R.4:** the system should have its own communication channel so that the status of the satellite can be known even if the satellite's communication module is faulty. **R.5:** the system should determine the attitude of the satellite as well as the tumbling rate. **R.6:** it should be possible to measure temperature at different locations of the satellite to validate the satellite's thermal system.

Chirper meets all the aforementioned design requirements and monitors the critical faults in the satellites as specified by NASA and others in the literature [1, 2, 14].

3 CHIRPER DESIGN

There are many challenges in designing a space-qualified Chirper because of the aforementioned requirements and many other constraints posed by the harsh space environment. In any case, a faulty Chirper (if it fails) should not damage a functional satellite. Even the voltage and current measurements of different subsystems must be isolated. Achieving this is challenging when it especially comes to isolated low DC voltage (0 to 48 V) measurement at high resolutions (for e.g., in steps of 1V). There is hardly any work in the literature that performs isolated voltage measurement for low DC voltages. Additional challenges come in the form of low power long-range communication, power storage (while bulk batteries cannot be used), and reliability. Taking into account the requirements listed in Section 2.2, we propose a novel design of Chirper.

The Chirper hardware is comprised of high reliability space-qualified components. These components are generally manufactured and tested for avionics, military, and space applications. They are robust to harsh environments such as extreme temperature, vibration, and vacuum like the space-grade components. While they can tolerate radiation in Low Earth Orbit (LEO), they support temperature range (-55 °C to 125 °C) as that of space-grade materials. They are also better than general COTS components (including industrial and automotive grade) in terms of reliability and failure rates.

3.1 Electronics

The block diagram of the Chirper is shown in **Figure 3**. The design consists of three main units: (i) Energy harvesting and power management; (ii) data processing and sensor unit, and (iii) communication unit. These units are explained in detail in the sequel.

3.1.1 Energy harvesting and power management. The Chirper is powered by space-grade solar cells – CTJ30 from CESI, each with

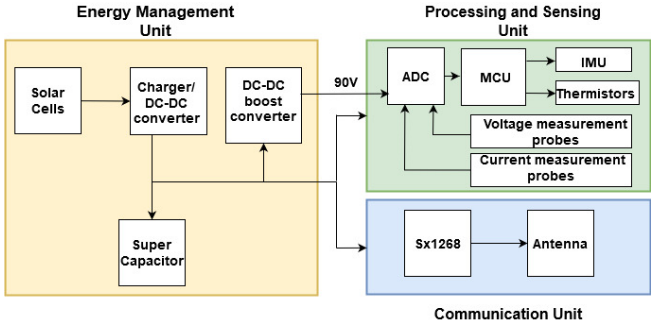

Figure 3: The block diagram of the Chirper showing three main units – energy management, processing, and communication unit

a dimension 2 cm × 2 cm that delivers a maximum of 2.4 V, 70 mA. This specific cell is chosen because of its high efficiency of 28.5 % for such a tiny size. Alternatively, any other space-grade solar cell/cells can be used but it may have an impact on the amount of harvested energy. Though Chirper is functional with one solar cell, we prefer to have at least one solar cell on each side of the satellite so that continuous energy will be available irrespective of the attitude of the satellite. The solar cells power the entire electronics through a solar charger IC ADP5090 from Analog Devices that can simultaneously charge a supercapacitor as well as deliver 3.3 V to the rest of the system. As soon as the satellite is deployed and the Chirper's solar cells are illuminated, the supercapacitor starts charging and the entire electronics is powered up. The supercapacitor acts as an energy bank when the sunlight is not incident on the solar cell. It was quite a challenge to find a supercapacitor that is tiny, sustain in vacuum and can work in space. We chose Murata's DMT334R2S474M3DTA0 470 mF supercapacitor having the dimensions 2.1 cm × 1.4 cm × 3.5 mm because of its wide temperature range and robustness. Chirper is flexible to be mounted anywhere inside or outside a satellite, however, at least one solar cell mounted on the surface of the satellite is connected through wires to the Chirper.

3.1.2 Sensing and data processing. A low power space-qualified microcontroller MSP430FR5969-EP from Texas Instruments is used as the data processing unit. It operates at 16 MHz frequency. It supports up to 16 ADC channels to which the thermistors and isolated voltage and current measurement sensors or a combination of them can be connected. The principle and implementation of isolated voltage and current measurement units are explained in Section 4 in detail. Further, one I2C and SPI channel from the microcontroller is facilitated over the Micro DB-9 connector to connect any external sensors if required by the satellite manufacturer. A low power onboard miniaturized IMU ICM-20948 from Invensense equipped with a 3-axis accelerometer, 3-axis gyroscope, and 3-axis magnetometer is used to estimate the body tumbling rate and attitude of the Chirper, and in turn, the host satellite.

3.1.3 Communication. There are many design choices for the communication unit to transmit the signals. Techniques such as Frequency Modulation, Phase Modulation, and Amplitude Modulation

call for high RF transmission power (as high as 1 W) to cover the LEO altitude of 2000 km. As the harvested power is limited for the Chirper, we choose LoRa as the modulation technique to transmit the telemetry. Moreover, when the satellite is tumbling, if the Chirper's antenna is disoriented along with that of the satellite's, then the telemetry received may contain a low Signal to Noise Ratio (SNR). It is very crucial in such situations to decode the signals successfully. LoRa supports SNR as low as -20 dBm. This leaves us to go for Semtech's SX1268 chip as it has proven flight heritage. SX1268 supports RF frequencies between 410 MHz and 810 MHz to be tuned for transmission/reception and the maximum transmission power of 22 dBm. We tune it to the UHF amateur frequency (anywhere between 435 MHz, and 438 MHz as fixed by the International Telecommunication Union (ITU) for a satellite). In this frequency range, the data from the Chirper can be received by amateur radio enthusiasts[4] all over the world; they send the collected information to the manufacturer/owner so that they can take necessary action. We chose amateur frequencies because of two reasons: (a) When a satellite breaks down, it may not be in the visibility of the designated ground station. Thus, a network consisting of such radio enthusiasts around the globe will be handy when emergency telecommanding is needed; and (b) Multiple signal receptions by enthusiasts in the neighborhood can help in providing data integrity (and redundancy) during the intermittent and/or broken signal reception.

SX1268 supports both Frequency Shift Keying (FSK) and LoRa modulation schemes. FSK can also be employed on Chirper provided that the receiver antenna on the ground station must have very high gain to meet the link budget calculations. The selection of LoRa or FSK is left to the satellite manufacturer. For LoRa, we choose the spreading factor to be SF7 at 125 kHz bandwidth over SF12 to reduce the airtime. However, SF12 can be used to achieve longer communication range and better sensitivity compared to that of SF7 at the cost of bandwidth and air-time. The maximum payload size is limited to 222 bytes because of the chosen SF factor. However, there is no limitation for FSK.

Note that Chirper telemetry and the main satellite communication can co-exist and operate at the same time provided that both the units are not employing the same modulation technique on the same frequency band. If multiple satellites with Chirper mounted on them are in the field of view of a ground station, the chances of RF interferences are extremely low as the frequencies are allocated by ITU depending on the satellite orbit to avoid RF interference as much as possible.

A fixed dipole antenna of gain 0 dBi tuned for the aforementioned UHF range is used in Chirper for transmitting telemetry and also to monitor if the host satellite's communication module is working. This is an easy way to find out whether the communication subsystem is working, if so, at what power. It should be noted that an RF limiter is placed between the receiving path of SX1268 and the antenna to avoid saturation or damage to the chip because of RF coupling from the host satellite's high power RF transmission. An optional U.FL connector is also provided in the Chirper to connect an external antenna in case the Chirper is placed inside the satellite. The external antenna must be omnidirectional so that the ground station can receive the signals even when the satellite is tumbling. The overall power consumption of the Chirper is around 250 mW when transmitting at 22 dBm, and at most 125 mJ of energy is required to sense, process, and transmit once with LoRa (at 22 dBm) at SF7.

While we present the Chirper design and communication details for satellites in LEO, Chirper can also be mounted on satellites in Medium Earth Orbits (MEO) and higher. However, this comes with new requirements – all the components used must of space grade counterparts due to extreme temperature changes and radiations. Additionally, the ground station must have a very high gain antenna to receive the signals from Chirper even if the telemetry is on LoRa.

3.2 Solar cell configurations and Energy harvesting

The Chirper is powered by six individual solar cells that are connected in parallel to each other. The size of each solar cell should be as small as possible unless the availability of ample space. As the cells are miniaturized, the energy harvested from them is limited. This being the scenario, the Chirper needs to operate in all the instances, including the case when the solar cell is intermittently pointed towards the sun during the tumbling scenario. Therefore, it is necessary to analyze the harvested energy from all the solar cells in all the sun pointing conditions and optimize it for reliable measurement and data transmission. At the same time, sufficient energy should also be stored in the supercapacitor so that the Chirper can operate even during eclipse (when satellite is on the anti-sun side of the earth).

While the satellite orbit is known and so the tumbling rate (from IMU), it is possible to predict the attitude of the satellite with respect to the Sun to estimate the amount of energy that can be harvested at any instant. However, this requires additional sensors on board, such as a star or the sun sensors, to determine the sun angle. Alongside, Chirper needs to ensure continuous and accurate timekeeping without any clock drifts along with Sun-Earth visibility model stored onboard. Any reboot cycle on Chirper disturbs this timekeeping. To avoid the complexity of the algorithm and processing all these parameters on the microcontroller, we set an active period interval for the Chirper during which the measurements are made, and the telemetry is transmitted. The rest of the time, Chirper will be in sleep mode.

With a solar power model, we first explain why six solar cells are necessary, even though the Chirper can be operated with one cell.

Why six solar cells? Though Chirper can be powered using a single solar cell, we choose to mount at least one cell on each side (considering a more common cuboid satellite) of the satellite for energy harvesting. We explain the need for six solar cells by providing example configurations with five and two cells. Let us consider a scenario where five solar cells are mounted on each side of a cuboid satellite. Assuming that the satellite is not tumbling, there may be a case where the side without solar cell is pointing towards the sun continuously, as depicted in **Figure 4a**. Even if the satellite is tumbling in the direction indicated by yellow arrow in **Figure 4a**, sun rays are not incident on the any of the five solar cells.

[4]Radio amateurs are enthusiastic about space technology and they track satellites continuously.

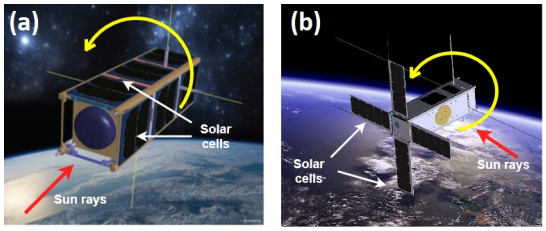

Figure 4: (a) Solar cells are mounted on five sides of the satellite. Only the side without solar cell is facing towards the Sun, (b) Deployable solar cells on a tumbling satellite. Yellow arrow shows the tumbling direction.

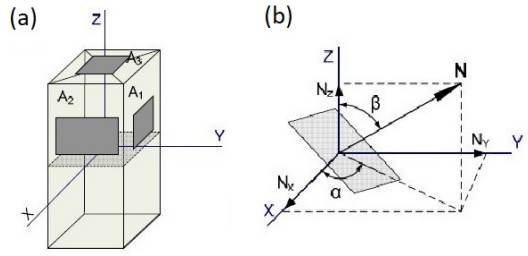

Figure 5: (a) Three solar cells mounted on three sides of a satellite. Any time, the maximum of three sides of a cuboid shaped satellite is visible to the Sun (b) The geometry of the solar cell when incident to the sunlight.

In such cases, no energy is harvested, and the Chirper is switched off until the sun rays are incident again. This gets worse as the solar cell count decreases. Let us consider another scenario, where solar cells are deployable as shown in **Figure 4b**. The tumbling direction (marked by the yellow arrow) and the incidence of sun rays are shown in the figure. Even in this case, the solar cells are not illuminated irrespective of whether the satellite is functional or not. Hence, if all the sides are mounted with at least one cell on each side, Chirper will always be powered. Thus a minimum of six solar cells is required to ensure the reliability of operation. However, the decision on the number of solar cells to be used is left to the satellite manufacturer.

Now, we proceed to provide a model for the amount of energy generated by the solar cell configuration at any time irrespective of whether the satellite is tumbling or not.

3.2.1 Energy harvesting. In this section, we provide a theoretical basis for estimating the total harvested power by six solar cells at any time. It is easy to estimate the total harvested power when the solar panel is at a constant incident angle with respect to the Sun. However, it is difficult to find the total power when the satellite is tumbling. We thus provide an analytical study to find the average minimum harvested power independent of the tumbling rate and/or orientation of the satellite. This is an important result that helps in designing the electronics on the Chirper.

At any time, for a tumbling cuboid satellite in any direction, at most three sides are pointing towards the sun. Hence, let us

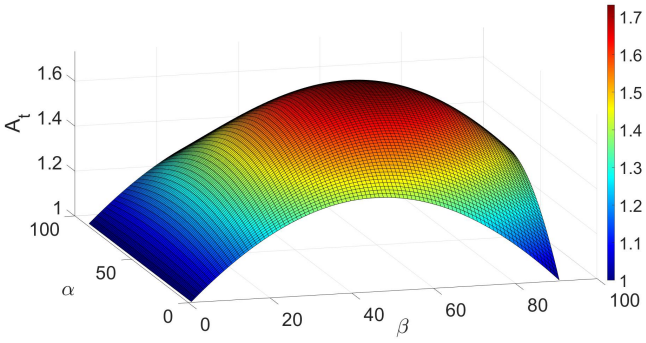

Figure 6: The total area of the three solar cells in parallel is a cosine function of the angle between the incident sun rays and the surface of the solar cell

consider three solar cells having equal area, each mounted on three sides of a tumbling satellite, as shown in **Figure 5a**. Let N be the normalized vector to each solar cell that is parallel to the Sun's incident rays as shown in **Figure 5b**. If N_x, N_y, and N_z are the three imaginary vectors along x, y, and z axes, then the amount of power generated for any cell at any time depends on the angles α and β, and the horizontal and vertical inclination of the cell with respect to the vector N. According to Lambert's Cosine law, the radiant intensity or luminous intensity observed from an ideal diffusely reflecting surface or ideal diffuse radiator is directly proportional to the cosine of the angle between the direction of the incident light and the normal to the surface [15]. Hence, the average power 'P' generated by a solar cell can be given as,

$$P = P_k A \eta, \tag{1}$$

where P_k is the solar constant and equals to $1367\, W/m^2$, A is the area of the cell that is incident to the sun rays, and η is the efficiency of the solar cell.

The total projected area, A_t, of all the cells combined in the direction of the Sun for 90°rotation is [15],

$$A_t = \int_0^{\pi/2} \int_0^{\pi/2} (A sin\beta cos\alpha + A sin\beta sin\alpha + A cos\beta) d\beta d\alpha. \tag{2}$$

$$\implies A_t = A\left(2 + \frac{\pi}{2}\right) \tag{3}$$

Note that the negative values of angles are discarded as the cell is illuminated for angles between 0 and $\frac{\pi}{2}$. Considering three solar cells, the average area A_{avg} of the cell on each side that is incident to the sun during tumbling is,

$$\frac{1}{A_{avg}} = \frac{1}{A_t} . \int_0^{\pi/2} \int_0^{\pi/2} d\beta\, d\alpha \implies A_{avg} = \frac{A_t}{\pi^2/4} \tag{4}$$

For all values of α and β in steps of 1° between 0 and $\pi/2$, the values of A_t are shown in **Figure 6**. From (2), we observe that the minimum and maximum values for A_t are 1 and 1.732, respectively.

Substituting (1) and (3) in (4), we get the average power P_{avg} generated during tumbling as,

$$P_{avg} = 1367 \text{ x } A\left(\frac{8 + 2\pi}{\pi^2}\right)\eta. \tag{5}$$

For the six cell solar configuration, we considered CTJ30 solar cells from CESI. The area of each cell is 0.0004 cm^2, and η = 28.5%. Substituting these in (5), there will be a minimum power of 155 mW harvested at any time irrespective of whether the satellite is tumbling or not.

3.2.2 Choosing the duty cycle. With the available harvesting power of 155 mW, let us choose an optimal duty-cycle period for operating the Chirper, thus minimizing energy consumption. The maximum eclipse duration for a LEO satellite is around 35 minutes [16] in its complete orbit of 2 hours (around 500 km altitude). During this period, that is when the satellite is on the anti-sun side of the earth, there is no energy harvesting. Hence, we need to ensure that the energy stored in the capacitor during the sunlit duration of 1 hour 25 minutes (=5100 s) lasts for at least 35 minutes of the operation of Chirper.

When the Chirper is turned ON, it collects the health parameters of the satellite, processes them, and then transmits them over LoRa communication unit. We call this an active period. The transmission duration (airtime) of LoRa depends on the spreading factor chosen and the transmission bandwidth. The spreading factor has to be wisely chosen as it impacts the link budget, in turn, the transmission distance. We choose SF7, 125 kHz bandwidth, and the maximum available transmission power of 22 dBm (contributing to the worst-case power consumption). The airtime for transmission of 222 bytes in SF7 is around 370 ms, which results in the total time required for the Chirper to sense, process, and transmit is around 500 ms. Hence, the energy consumption for one transmission (250 mW × 500 ms) is 125 mJ. For FSK, it is less due to short airtime ≈250 ms to transmit at 9.6 k baud rate. Hence, we consider the worst case of 125 mJ per active period. When the Chirper is not active, the microcontroller is in sleep mode, and the rest of the electronics are turned OFF to consume only 1 mW power.

If P_A = 250 mW is the active mode power and P_S = 1 mW is the sleep mode power of the Chirper, the duty-cycle can be represented as $t_{\text{ON}} + t_{\text{OFF}}$ which is nothing but the total orbital period, i.e., 2 hours. t_{ON} is the duration equivalent to TN_t, where T is the duration of transmission and N_t is the number of transmissions in one orbit. t_{OFF} is the duration when Chirper is in sleep mode. Now, let us calculate the number of active periods, i.e., the regular intervals at which there will be a transmission. We start by budgeting the energy harvested and energy spent in one orbit. We know that energy harvested during the sunlit period, $E^{(t)}$,

$$E^{(t)} \geq E^s + E^e, \tag{6}$$

where, E^s is the energy spent during the sunlit period and E^e is the energy spent during an eclipse. Further, we know that energy harvested during the sunlit period is 155 mW x 5100s = 790.5 J. Now,

$$\begin{aligned} E^s &= P_A * t_{\text{ON}} + P_S * t_{\text{OFF}}, \\ &= 0.125N_t + 5.1 - 0.0005N_t \text{ Joules}. \end{aligned} \tag{7}$$

Similarly,

$$\begin{aligned} E^e &= P_A * t_{\text{ON}} + P_S * t_{\text{OFF}}, \\ &= 0.125N_t + 2.1 - 0.0005N_t \text{ Joules}. \end{aligned} \tag{8}$$

Substituting (7) and (8) in (6), we get $N_t \leq 3156$. This means that there can be a maximum of 3156 transmissions in a single two hour orbit period, i.e., once in every 3 s before the harvested energy is completely exhausted.

However, this can be increased to 30 s as the nominal visibility period[5] of a satellite in LEO varies between 30 s to 15 minutes [17]. Hence, the Chirper must transmit at least once in 30 s to ensure that the ground station receives a packet in all the visible passes.

3.2.3 Capacitance of the supercapacitor. When the satellite is in eclipse, supercapacitor is the only energy source. The capacitance of the supercapacitor that stores the harvested energy depends on the eclipse duration, the duty cycle period, and the energy consumption of the Chirper. Since we set the duty cycle period to be 30 s, and substituting N_t = 70 (70 transmissions in 35 minutes) the total energy required for the Chirper to be functional during an eclipse is 10.82 J. The capacitor's maximum charge voltage is 4.2 V. Hence, the capacitance required is 1.22 F. We choose Murata's three DMT334R2S474M3DTA0 470 mF capacitors in parallel summing up to the total capacitance of 1.41 F. These capacitors are charged fully when the satellite is on the sunlit side.

4 ISOLATED DC VOLTAGE AND CURRENT MEASUREMENT

In this section, we explain the design and working principle of the proposed isolated DC voltage and current measurement techniques. Before we proceed with our solution, we present the design choices available to measure DC voltage without any electrical contacts.

4.1 Design choices for low voltage DC voltage measurement

There are a limited number of options available for isolated DC voltage measurement.

1. Isolated DC-DC converters: The easiest way to measure DC voltage with isolation is using DC-DC converters that offer a feature of isolation. The isolation is based on transformers or LED - photodiodes. This system is not only bulky but also requires one part of the system to be electrically connected to the parent satellite. Any electrical short in the system can shut down the entire satellite.

2. Surface potential measurement: Surface potential sensors such as the EFS series from TDK measure DC voltage on the surface of a conductor. These sensors provide complete isolation as they can be placed up to 10 cm away from the conductor, and mainly, there is no electrical contact required. However, these sensors are expensive and intended for detecting DC voltages over large ranges (0 to 1000 V). Generally, they provide a measurement resolution of 10 V which is not sufficient to measure the DC bus voltage (0-48 V) of a satellite. At least a resolution of 1 V is necessary as the bus voltage varies between 44 V to 48 V during nominal operation.

3. Capacitance on the cable insulation: There are a few works in the literature where coupling capacitance formed between the conducting wire and its insulation is measured to estimate the voltage. However, this technique is widely used for AC voltage measurements or to detect only the presence of high voltage DC voltage.

[5]The visibility period is the duration for which the satellite is visible at a particular ground station. This period depends on the geographical location of the ground station, orbit of the satellite, and the maximum angle at which the satellite is visible in that particular satellite pass.

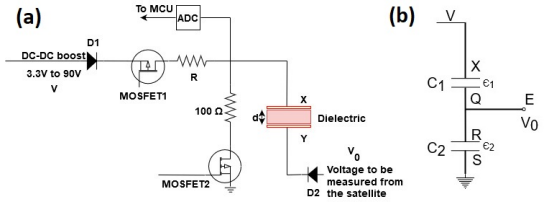

Figure 7: (a) Circuit diagram of the proposed low DC voltage measurement technique; (b) Working principle of the proposed voltage measurement model.

None of these existing techniques can be used in our application as either they do not provide complete isolation, or they do not provide the measurement resolution required by the Chirper. The unavailability of an isolated DC voltage measurement technique that suits the requirements of the Chirper motivated us to develop a new capacitive based isolated DC voltage measurement technique.

4.2 DC voltage measurement

The proposed technique to measure DC voltage on the main power bus of the satellite and other subsystems is based on the capacitance theory. A simple capacitor is created using two aluminum plates X and Y, and a dielectric material sandwiched between them as shown in **Figure 7a**. Plate X is connected to a DC power supply on the Chirper. Plate Y of the capacitor is connected to the voltage line that needs to be measured on the satellite. The charging or discharging time of the capacitor depends on the voltage on the plate Y that can be measured by the microcontroller on the Chirper .

Working principle: To explain the working principle of the measurement technique, let us consider two capacitors C1 and C2, with dielectric 'ϵ_1' and 'ϵ_2' respectively, in series as shown in **Figure 7b**. A potential of 'V' is applied between terminals P and S. The charge stored on each capacitor is equal to capacitance × voltage across its parallel plates. Let terminal 'E' be a tap from the junction point of two capacitors. If a potential 'V_0', such that $V_0 < V$, is applied on terminal 'E', then the charge stored across C1 and C2 varies proportionally to V_0. If V_0 is the voltage under measurement, then it can be calculated by measuring the charge across C1 during its charge and discharge cycles. To ensure isolation, we modify this circuit as shown in **Figure 7a**, where the dielectric medium of C2 is replaced by vacuum, and plates Q and R are merged to form plate Y. Plate X is connected to a DC power supply V through a resistor 'R'. The charging/discharging of the capacitor is controlled by the microcontroller using two MOSFETS as shown in the figure. Both the Chirper and the host satellite will share a common ground.[6] A non-conductive dielectric medium is sandwiched between plates X and Y. Since there is no electrical contact between plate X and plate Y, the Chirper and the voltage line to be measured are isolated. As a safety feature, two diodes D1 and D2 make sure that there will not be any reverse current flow to the Chirper as well as the satellite voltage line. The capacitance 'C' of the capacitor is given by,

$$C = \frac{A\epsilon_0\epsilon_r}{d}, \tag{9}$$

where A is the area of plates X and Y, ϵ_0 is the absolute permittivity, a constant, and ϵ_r is the relative permittivity of the dielectric used between the plates, and d is the distance between the plates.

The area of the plates must be as small as possible for miniaturizing the system. However, this leads to a low capacitance, leading to less charging and discharging time that may be in the order of nanoseconds. Such a low-resolution time measurement is not possible with a 16 MHz MSP430 microcontroller. Hence, the charging/discharging time must be set to an extent that it can be measured by the microcontroller. Additionally, to avoid noise and offsets in the measurement, the capacitance between the plates should be much larger than the stray capacitances of the PCB traces and cables used for voltage measurement. Decreasing the distance between the plates to increase the capacitance can be an option, however, this is not suggestible as more gap between the plates ensures good isolation. From (9), the only way to increase the capacitance is by choosing a material with a high dielectric constant. Additionally, the charging time can be controlled by the resistor 'R'.

For a fixed capacitance 'C', the electric charge 'Q' stored in the dielectric is proportional to the voltage difference between plate X and Y. That is, $C = \frac{Q}{V - V_0}$, where V is the charging voltage applied on plate X and V_0 is the voltage on plate Y that needs to be measured. It should be noted that the charging voltage must be greater than V_0. Hence, if the maximum voltage that needs to be measured is 48 V, then $V > 48$ V. As the Chirper operates at 3.3V, a step-up converter needs to be used to boost the 3.3V input above V_0. We use LT3482 from Analog Devices to boost the input voltage of 3.3 V to 90 V, its maximum capability. The instantaneous voltage 'V_C' across the capacitor at time 't' is given by,

$$V_C = V\left(1 - e^{\frac{-t}{RC}}\right). \tag{10}$$

Initially let us assume a case where the plate Y is at the zero potential ($V_0 = 0$) and the capacitor is completely discharged. Let t_0 be the time taken to charge the capacitor to V volts (it is 90 V in our case) from zero. This is always a constant. In another case, when $V_0 > 0$, plate Y is at a potential of V_0 initially. As soon as MOSFET 'M1' is switched ON and 'M2' is switched OFF, the capacitor starts charging towards V from V_0. Let the time taken to charge the capacitor from V_0 to V be t_v. The difference between the time 't_0' taken to charge the capacitor from 0 to V, and the time 't_v' taken to charge the capacitor from V_0 to V (where $0 < V_0 < V$) is equal to the time taken to charge the capacitor from 0 to V_0, i.e, $t_0 - t_v$. Hence, from (10),

$$V_0 = V\left(1 - e^{\frac{-(t_v - t_0)}{RC}}\right). \tag{11}$$

t_v is measured from the time at which 'M1' is turned ON until the capacitor is fully charged. The voltage level on the plate X is measured by the microcontroller using a high voltage analog comparator as shown in **Figure 7**. When M1 is turned ON and M2 is OFF, one plate of the capacitor is at V_0, and another at V. Hence, the capacitor tends to charge from V_0 to V. It should be noted that both M1 and M2 are turned OFF when voltage on plate X

[6] all the subsystems of the satellite are connected to the electrical ground and the satellite structure to avoid the static charge that can arise due to charged plasma and cosmic rays in space

is being measured. Once t_v is measured, the capacitor is discharged by turning 'M2' ON and 'M1' OFF. We perform this cycle every 1 ms, and measure the capacitor voltage using ADC. Note that the capacitor is charged to V at $t = \infty$ according to (9). Hence, we consider the full charge condition to appear at 99.3% of V, which requires 5 times the time constant.

The nominal area of each capacitor plate is chosen to be around 1 cm^2 at a distance of 0.5 mm with a thin conjugated polymer as a dielectric medium having $\epsilon_r = 800$. This results in the capacitance of C = 1.42 nF between A and B. We choose R = $20M\Omega$ to set a charging time of 142 ms that can be easily measured by the 16 MHz microcontroller. However, we do not impose any restriction on the value of the charging resistor, size of the plate, the distance between the plates, and the dielectric property of the material. The goal is to have proper isolation while the capacitor is miniaturized.

4.3 DC current measurement

The isolated DC measurement is straightforward. We adapt the existing non-intrusive method of estimating the current flow in the current-carrying wire. According to Ampere's law, the magnetic field generated around the wire is proportional to the current flowing through it. In other words, $B = \frac{\mu_0 \mu_r I}{2\pi r}$, where B is the magnetic flux density, μ_0 is the free space permeability, a constant, μ_r is the material permeability which is nearly unity for air, I is the current flowing through the wire and r is the distance between the sensor and the wire. We use a TLE4997E2 hall effect sensor, placed in the air gap of a flux concentrator. The hall effect sensor provides voltage output, proportional to the magnetic flux around it. This method provides complete galvanic isolation.

5 EVALUATION

We evaluated the performance of Chirper in different scenarios - (i) the proposed DC voltage measurement technique was validated with simulation as well as real-time voltage measurements. (ii) the entire Chirper was mounted on a test system, and all the possible tests were conducted along with Chirper in a space laboratory. (iii) the Chirper was mounted on a helium balloon to test the line of sight communication and mimic tumbling scenario. In all these cases, we conduct different tests on the Chirper. In this section, we first provide the simulation results of the dc voltage measurement tests followed by tests on the satellite and balloon launch tests.

5.1 Simulation

The validation of the proposed DC measurement technique was done with simulation on OrCAD and pSpice. We created an equivalent charging and discharging circuit of the proposed voltage measurement technique as shown in **Figure 8**. With this, we validated (11) for different values of V_0. As an example, we present our simulation for one case where the voltage to be measured $V_0 = 48$ V. We consider two steps as explained earlier- (i) to measure t_0, V_0 was set to 0 V initially. This is one time calculation; (ii) V_0 was set to 48 V, and the capacitor was charged with $V = 90$ V. R1 was set as 20 MΩ and capacitance to 1.42 nF as mentioned in Section 4.2. The pSpice simulation results are shown in **Figure 9**. According to simulation results, the time taken to charge the capacitor from 0 V to 90 V was 0.142 s, and the time taken to charge from 48V to 90V was 0.12035 s. Let us assume that $V0$ is unknown. Now, using (11), we can calculate $V_0 = 48.007$ V. Thus, the simulation verifies our model.

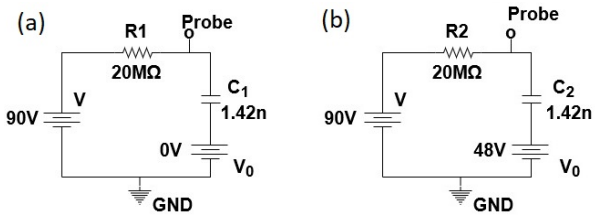

Figure 8: Equivalent circuit of our proposed DC voltage measurement method; (a) $V_0 = 0$ (b) $V_0 = 48$ V.

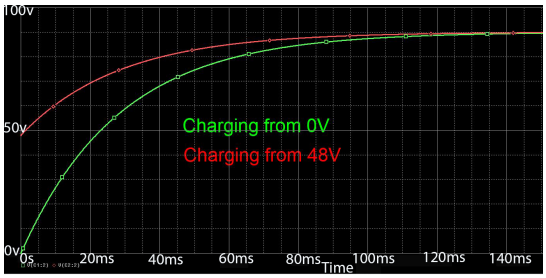

Figure 9: Simulation of capacitor charging.

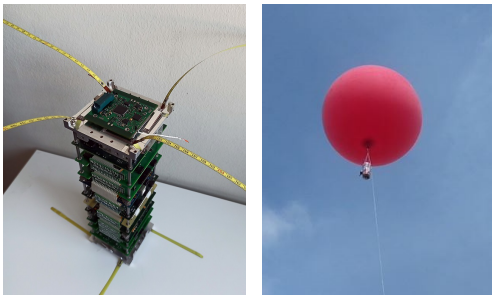

(a) **(b)**

Figure 10: (a) Example of the mounting of Chirper on a nanosatellite (b) Chirper tied to a helium balloon

5.2 Chirper on a real space-system

The Chirper can be mounted on top of a space system, e.g., a nanosatellite as shown in **Figure 10a**. Chirper was powered by its own dedicated six solar cells (not shown in the figure). Multiple voltage and current measurement probes were connected across the different subsystems of the satellite. A few thermistors - PS103J2 from LittleFuse placed at different locations (including on the satellite body and a few critical chips on the PCBs) were connected to ADC of the Chirper using wires to measure temperature. Extensive tests were performed on the Chirper. Several table-top equipment such as Tektronix DMM4020 digital multimeter were used to validate the voltage and current measurements done by the Chirper.

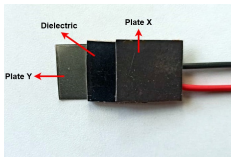

(a)

(b)

Figure 11: (a) Voltage probe (b) Current probe

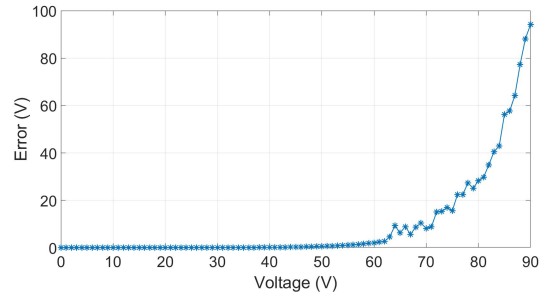

(a)

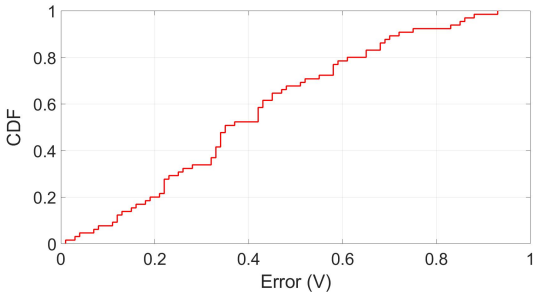

(b)

Figure 12: (a)Error in measured voltage. (b) CDF of error in measured voltage.

Figure 11 shows our experimental voltage and current measurement probes. The capacitor plates of the voltage probe were covered with kapton tape (which is not shown here) to ensure proper isolation and safety. The outer casing of the current probe was taken from Winson WCS1700 current measurement sensor. We replaced their hall-effect sensor with TLE4997E2 as it was not qualified for space. The wire carrying current that had to be measured was passed through the center hole of the probe. The tests performed were as follows.

5.2.1 Laboratory tests. The accuracy of the proposed voltage measurement technique was tested using a function generator. Varying DC voltages from 0V to 90V in steps of 1V was applied on a resistor load with variable resistance up to 100 kΩ. Using the measurement probes, the voltages and currents for different combinations were measured by the Chirper. **Figure 12a** shows the absolute values of error in voltage measurement for one channel. We observe from the figure that the error curve is exponential. This is because, when the

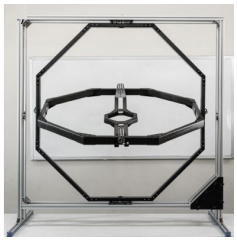

Figure 13: Commercially available (a) Solar simulator with lamp and (b) 3-axis rotation mechanism shown here for clarity. The photograph of the actual large-scale test setup is not permitted to be reproduced here.

difference between the charging voltage 'V' (see (11)) and the voltage to be measured 'V_0 is high, the capacitor takes more time to get charged. This time can be easily measured by the microcontroller. However, when V is very close to V_0, the capacitor will be quickly charged to full as one of the plates (plate Y in **Figure 7**) of the probe is already at V_0. For example, in our setup, the measurement error was within 1 V, for voltage upto $V = 60$ V. Beyond that, the error increases as the charge–discharge cycle of the capacitor is very short. Hence, depending on the measurement accuracy required and the maximum voltage that needs to be measured, the charging voltage V for the Chirper needs to be set. In our case, we choose $V = 90$V as most of the satellites have the bus voltage of 48V. The current measurement error was almost constant throughout the measurement range irrespective of the current passing through the wire. The maximum error observed was 62 mA. Irrespective of the number of voltage/current channels used for measurement, the error plot for each channel is similar to the one in **Figure 12a**. Moreover, each measurement channel is independent of each other and isolated.

Figure 12b shows the CDF of voltage measurement errors for $V_0 = 0$V to 50V while $V = 90$ V. We observe that 90% of the time the error is within 0.8 V and the maximum error observed was 0.9 V.

5.2.2 Energy harvesting. The Chirper mounted on a 3-axis rotation mechanism was subjected to the solar simulator to test the amount of energy harvested. An example of a solar simulator is shown in **Figure 13a**. The simulator produces luminescence equivalent to 1 Sun luminosity. The Chirper mounted on a 3-axis rotating mechanism FFT Gyro-450 [18] (which is usually used to test drones) from Eureka Dynamics is shown in **Figure 13b**, and it was placed in front of the solar simulator. The 3-axis rotation of the satellite was facilitated by PC based software and the emulated sunlight was made incident on the satellite. As solar cells were placed on all six sides of a test system to power the Chirper, irrespective of the tumbling direction or speed, the Chirper could harvest at least 145mW of power. This almost falls in line with the theoretical value 155 mW as mentioned in Sec 3.2. Voltage lines with different potentials - 3.3V, 5V, 7.2V, 8V, and 12V were emulated and were measured using Chirper. The required current measurement range was 0A to 1.5A. The results obtained were similar to the ones during lab tests.

Apart from the above tests, the Chirper has undergone environmental tests required by the launch providers - high vibration level and thermo-vacuum cycles. Our Chirper passed all the tests.

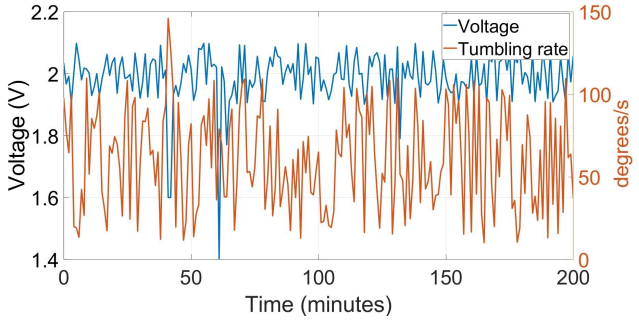

Figure 14: Voltage generated by the solar cell during tumbling

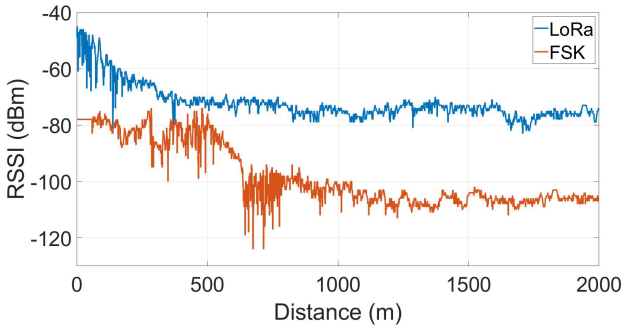

Figure 15: RSSI of the received signal from the balloon

5.3 Chirper on a high altitude balloon

The Chirper was launched on a helium balloon up to 2 km distance from the ground station receiver to emulate the tumbling scenario and validate the communication range. The Chirper along with a single CTJ30 solar cell from CESI was tied to the balloon and left hanging as shown in **Figure 10b**. As the balloon went up, it started tumbling and drifted due to the wind. The tumbling speed was calculated using IMU. The measured harvested voltage, current, and the tumbling rate were sent to the ground on LoRa (SF7, 125kHz), as well as with FSK every five seconds. The transmission frequency was set to 436 MHz and the transmission power on the Chirper was set to 22 dBm in both the cases. A -2 dBi monopole antenna was used on the Chirper. The communication packet size was set as 14 bytes.

5.3.1 Solar cell voltage vs tumbling. The voltage generated by the solar cell at different tumbling rates for 200 minutes of flight is shown in **Figure 14**. The voltage is averaged over one minute measurements. Irrespective of the tumbling direction/rate, the solar cell was incident on the sun rays most of the time and it generated sufficient power for the Chirper to operate even with a single solar panel. However, at some instances, for e.g., around 60th minute, the solar cell voltage dropped instantaneously. This is because, the solar cell was under the shadow of the balloon and the sunlight was not incident on the cell at 90°. As there was no attitude control on the balloon, the tumbling rate was very high – as high has 146°/s as shown in **Figure 14**. However, in an actual satellite, the tumbling rate will be much less than 146°/s. Thus this experiment depicted the occurrence of the worst-case scenario. This experiment also validates that the Chirper can be functional even with a single solar cell; as discussed earlier, six solar panels would help in case the orientation is not proper.

5.3.2 Communication– LoRa vs FSK. The data transmitted by the Chirper on the balloon was received on the ground using a custom designed SX1268 board and 5 dBi yagi antenna. The RSSI obtained at different distances for both LoRa (SF7) and FSK is shown in **Figure 15**. It is known that at the same transmission power, LoRa outperforms FSK over distance. This is evident from **Figure 15**. Though the distance between the receiver of ground and the balloon went up to 2 km, we extrapolated the obtained RSSI results up to 2000 km - the outer edge of Low Earth Orbit. As per Friis transmission equation, we could get the extrapolation result as -129 dBm for 2000 km where LoRa chip (whose receiver sensitivity is -136 dBm) can decode the messages successfully. However, this is not feasible with FSK at the aforementioned power and antenna gains. Indeed, the communication distance can be increased further by operating LoRa with higher spreading factors such as SF12 at the cost of huge bandwidth and longer airtime (more than 1.6 s to transmit 14 b at 125 kHz). However, the selection of physical layer, spreading factor, transmission bandwidth, and antenna gains are up to the satellite or parent space system manufacturer.

6 RELATED WORK

In this section, we list relevant works in the literature that are close to a fault monitoring system such as Chirper.

Fault-monitoring systems in terrestrial applications are not new. There are ample works in the literature that concentrate on supervising the critical systems for failures [19–22]. Most of them are either software based where failures are detected based on the abnormal data from the sensor units, or they are contact based where there will be an electrical contact between the measurement module and the target hardware. These solutions cannot be used on satellites as isolation is a necessary requirement. Indeed there are a few isolated voltage measurement techniques, where the voltage on a current carry line is measured without having any electrical contact. However, these target high voltage AC measurement using capacitive technology, wherein the coupling capacitance formed between the current carrying conductor and the cable insulation is measured. This capacitance is mapped to the voltage on the conductor [23–26]. TDK released a surface potential sensor to measure high voltage DC (0 - 1000 V) without any contact. The sensor can be placed as far as 10 cm from the surface of the conductor on which the voltage has to be measured [27]. The sensor has a resolution of only 10 V and the integration is complex because of the placement requirements.

Apart from software, the most common approach to fault detection and identification is hardware redundancy. If one of the subsystems fails, then its redundant part starts functioning. Having redundancy increases the reliability of the system but it may not identify the fault. Further, many satellites that failed in the last two decades had redundancy in their subsystems [1, 2]. T. Yairi et al., proposed a novel anomaly detection method for spacecraft systems based on data-mining techniques. [3]. Data mining provides tighter

bound to the limits. The solution does not include any additional hardware on the satellite but mining is done on the housekeeping data obtained from the satellite. The monitoring process is completely data-driven. Similarly, S. Bottone et al., present a novel technique to diagnose and predict the failure for a satellite subsystem using Bayesian network and probabilistic approaches [4]. The technique needs to have prior knowledge of the sensor data and it is completely data-driven. A satellite health monitoring system that reduces the need for hardware redundancy is proposed by R. H. Chen et al [5]. The proposed technique uses a modeled dynamic relationship between system inputs and measured system outputs to form a residual process that is used for detecting and identifying faults. The monitoring algorithm resides on the On-Board Computer of the satellite and completely rely on the data obtained from the satellite.

Health monitoring and fault detection in embedded systems has a lot of literature but they cannot be employed as is for the following reasons.

(1) Most of the existing methods for monitoring the heath of satellites are based on data analytics that employ the historical data received from the satellite. There may be cases, such as in GSAT 6A, wherein specific commands have to be up-linked to the satellite immediately when the the subsystems are in a particular state in case of issues [7]. The existing software and data statistical approaches may not be beneficial in this case. Alongside, conventional fault detection methods generally require a tremendous prior knowledge on the system behavior for each satellite, whereas that kind of knowledge is not always obtained easily beforehand. For example, a perfect dynamics model for simulating all the failure cases is too expensive to prepare for each satellite. To this end, we present a new independent and isolated system for monitoring the heath of a satellite. Though the notion of Chirper is not new and the fault monitoring systems do exist in the embedded systems domain, Chirper revisits it in a new, isolated, and reliable approach.

(2) Re-use of knowledge from past missions is also limited because each spacecraft is usually more or less different from past ones. Another reason is that these methods can grasp only limited aspects of overall spacecraft system behavior. For example, limit-sensing examines only upper and lower bounds of individual sensor values, and dynamics simulation can be performed on only several subsystems such as attitude control systems.

(3) The existing fault monitoring techniques are not completely isolated. Even if there is a separate health monitoring subsystem, they are electrically connected to the satellite and rely on satellite's main power. Any failure in the satellite main power system affects the health monitoring module.

(4) High resolution isolated voltage measurement is necessary to monitor the voltage levels on different subsystems of a satellite. For instance, the functional solar panel voltage or a battery can vary between 9V and 13.1V, hence a measurement resolution of 1V would suffice. To the best of our knowledge, there is no isolated DC voltage measurement that can provide a resolution of 1 V measuring low voltages in the range 0 to 48 V. Chirper provides the DC voltage measurement accuracy of 1V, hence we set the resolution to be 1V. However, the proposed measurement technique can be improvised to get accuracy in millivolts by choosing an appropriate capacitor plate material and dielectric medium.

7 CONCLUSION

In this work, we presented a novel and complete design of a space system called Chirper. Chirper is a low-power, independent, low-cost system that monitors the health of a large space system (parent), such as, satellites, when mounted on them. The name Chirper symbolizes the sound a bird makes when it faces a dangerous situation. We explicated the need, requirements, and challenges in designing and developing such systems. SpaceWorks estimates that up to 2600 small satellites (in the mass range 1-50 kg) will be launched over the next 5 years, thus a system like Chirper will be highly sought after. We also provided a new approach to measure the DC voltage in a completely isolated way. Further Chirper measure current flow, orientation, and the tumbling rate of the parent. We built a Chirper, tested its suitability for space launch, and evaluated its capabilities to collect health parameters in state of the art simulators. We also launched Chirper on a helium balloon to test it in a highly unstable environment and received both LoRa and FSK signals. Additionally, Chirper is capable of receiving telecommands from the ground station and communicate with the subsystems (of course, if wireless connectivity between the parent and the Chirper is enabled). Chirper can be used not only in space applications but also in terrestrial applications. Now, with all the space launch-related requirements fulfilled, it is expected that Chirper will be onboard a space system in a few months.

REFERENCES

[1] NASA. (2019) Small-satellite mission failure rates. [Online]. Available: https://ntrs.nasa.gov/archive/nasa/casi.ntrs.nasa.gov/20190002705.pdf

[2] "A study of on-orbit spacecraft failures," *Acta Astronautica*, vol. 64, no. 2, pp. 195 – 205, 2009.

[3] T. Yairi, Y. Kato, and K. Hori, "Fault detection by mining association rules from housekeeping data," in *In Proceedings of the 6th International Symposium on Artificial Intelligence, Robotics and Automation in Space*, 2001.

[4] S. Bottone, D. Lee, M. O'Sullivan, and M. Spivack, "Failure prediction and diagnosis for satellite monitoring systems using bayesian networks," in *MILCOM 2008 - 2008 IEEE Military Communications Conference*, Nov 2008, pp. 1–7.

[5] R. H. Chen, H. K. Ng, J. L. Speyer, L. S. Guntur, and R. Carpenter, "Health monitoring of a satellite system," *Journal of Guidance, Control, and Dynamics*, vol. 29, no. 3, pp. 593–605, 2006. [Online]. Available: https://doi.org/10.2514/1.15012

[6] L. A. Times. (2019) The latest lost satellite is now space junk that could put other spacecraft at risk. [Online]. Available: https://www.theverge.com/2019/4/19/18507439/intelsat-29e-geostationary-orbit-satellite-failure-space-debris

[7] S. Now. (2018) Isro loses contact with new communications satellite. [Online]. Available: https://spaceflightnow.com/2018/04/03/isro-loses-contact-with-new-communications-satellite/

[8] NASA. (2014) Cots components in spacecraft systems: Understanding the risk. [Online]. Available: https://www.nasa.gov/sites/default/files/atoms/files/cots.pdf

[9] S. Narayana, R. V. Prasad, V. S. Rao, and C. Verhoeven, "Swans: Sensor wireless actuator network in space," in *Proceedings of the 15th ACM Conference on Embedded Network Sensor Systems*, ser. SenSys '17, 2017.

[10] M. E. S. Sally Cole. (2020) Small satellites increasingly tapping cots components. [Online]. Available: http://mil-embedded.com/articles/small-tapping-cots-components/

[11] Starlink. (2020) Starlink. [Online]. Available: https://www.starlink.com/

[12] S. News. (2019) Digitalglobe loses worldview-4 satellite to gyro failure. [Online]. Available: https://spacenews.com/digitalglobe-loses-worldview-4-satellite-to-gyro-failure/

[13] ESA. (2001) Ers-2 goes gyro-less. [Online]. Available: https://www.esa.int/Enabling_Support/Operations/ERS-2_goes_gyro-less

[14] G. A. Landis, "Tabulation of power-related satellite failure causes," in *11th International Energy Conversion Engineering Conference*, 2013.

[15] M. Oredsson, "Electrical power system for the cubestar nanosatellite," 2010.

[16] Y. Borthomieu, "14 - satellite lithium-ion batteries," in *Lithium-Ion Batteries*, G. Pistoia, Ed. Amsterdam: Elsevier, 2014, pp. 311 – 344. [Online]. Available: http://www.sciencedirect.com/science/article/pii/B9780444595133000145

[17] S. Narayana, R. Muralishankar, R. V. Prasad, and V. S. Rao, "Recovering bits from thin air: Demodulation of bandpass sampled noisy signals for space iot,"

in *Proceedings of the 18th International Conference on Information Processing in Sensor Networks*, ser. IPSN '19. Association for Computing Machinery, 2019, p. 1–12.

[18] E. Dynamics. (2020) Fft gyro 600 pro. [Online]. Available: https://eurekadynamics.com/fft-gyro-600/

[19] V. Chatzigiannakis and S. Papavassiliou, "Diagnosing anomalies and identifying faulty nodes in sensor networks," *IEEE Sensors Journal*, vol. 7, no. 5, pp. 637–645, 2007.

[20] T. Chakraborty, A. U. Nambi, R. Chandra, R. Sharma, M. Swaminathan, Z. Kapetanovic, and J. Appavoo, "Fall-curve: A novel primitive for iot fault detection and isolation," in *Proceedings of the 16th ACM Conference on Embedded Networked Sensor Systems*, ser. SenSys '18. New York, NY, USA: Association for Computing Machinery, 2018, p. 95–107.

[21] B. Sheng, Q. Li, W. Mao, and W. Jin, "Outlier detection in sensor networks," in *Proceedings of the 8th ACM International Symposium on Mobile Ad Hoc Networking and Computing*, ser. MobiHoc '07. New York, NY, USA: Association for Computing Machinery, 2007, p. 219–228.

[22] F. Koushanfar, M. Potkonjak, and A. Sangiovanni-Vincentelli, "On-line fault detection of sensor measurements," in *SENSORS, 2003 IEEE*, vol. 2, 2003, pp. 974–979 Vol.2.

[23] D. Lawrence, J. S. Donnal, S. Leeb, and Y. He, "Non-contact measurement of line voltage," *IEEE Sensors Journal*, vol. 16, no. 24, pp. 8990–8997, 2016.

[24] P. S. Shenil, R. Arjun, and B. George, "Feasibility study of a non-contact ac voltage measurement system," in *2015 IEEE International Instrumentation and Measurement Technology Conference (I2MTC) Proceedings*, 2015, pp. 399–404.

[25] S. Wei, L. Zhang, W. Gao, and Z. Cao, "Non-contact voltage measurement based on electric-field effect," *Procedia Engineering*, vol. 15, pp. 1973 – 1977, 2011, cEIS 2011. [Online]. Available: http://www.sciencedirect.com/science/article/pii/S1877705811018698

[26] A. Delle Femine, D. Gallo, C. Landi, A. Lo Schiavo, and M. Luiso, "Low power contactless voltage sensor for low voltage power systems," *Sensors*, vol. 19, no. 16, 2019. [Online]. Available: https://www.mdpi.com/1424-8220/19/16/3513

[27] TDK. (2020) Surface potential sensors efs series. [Online]. Available: https://product.tdk.com/info/en/products/sensor/sensor/surface-potential/technote/tpo/index.html